A Quadratic Serendipity Finite Volume Element Method on Arbitrary Convex Polygonal Meshes

Yanlong Zhang[1,2,*]

[1] *Graduate School of China Academy of Engineering Physics, Beijing, 100088, P.R. China.*
[2] *Institute of Applied Physics and Computational Mathematics, Beijing, 100088, P.R. China.*

Abstract. Based on the idea of serendipity element, we construct and analyze the first quadratic serendipity finite volume element method for arbitrary convex polygonal meshes in this article. The explicit construction of quadratic serendipity element shape function is introduced from the linear generalized barycentric coordinates, and the quadratic serendipity element function space based on Wachspress coordinate is selected as the trial function space. Moreover, we construct a family of unified dual partitions for arbitrary convex polygonal meshes, which is crucial to finite volume element scheme, and propose a quadratic serendipity polygonal finite volume element method with fewer degrees of freedom. Finally, under certain geometric assumption conditions, the optimal H^1 error estimate for the quadratic serendipity polygonal finite volume element scheme is obtained, and verified by numerical experiments.

AMS subject classifications: 65N08, 65N12

Key words: Quadratic serendipity polygonal finite volume element method, arbitrary convex polygonal meshes, Wachspress coordinate, unified dual partitions, optimal H^1 error estimate.

1 Introduction

Due to the local conservation property, finite volume element method (FVEM) is a popular method for numerical simulation, and has been researched extensively in the last decades (e.g. [1–18]). At present, the linear FVEM on triangular and quadrilateral meshes has a relatively complete theory system, such as coercivity results, H^1 and L^2 error estimates. However, the research of quadratic FVEM is more difficult than linear scheme, then we give a brief review for the development of quadratic FVEM. For the quadratic FVEM on triangular meshes, there are plenty of schemes (e.g. [1–6])

based on different dual partitions with two parameters α and β. The coercivity of these schemes are almost established under certain minimum angle conditions, but up to now, only one scheme proposed in [5] is unconditionally stable. Moreover, for the existing schemes, there is only one scheme which has been proved that it has both the optimal H^1 and L^2 error estimates in [4]. Based on the existing coercivity results for the quadratic scheme in [4], it is not unconditionally stable, and how to remove the minimum angle condition is still an open and expectant problem. For the quadratic FVEM on quadrilateral meshes, the scheme [7] obtained the optimal convergence rate in H^1 norm for rectangular meshes, and the scheme [8] reached similar result for h^2-parallelogram meshes. But L^2 convergence rates of them are all not optimal. By using the optimal stress points to construct dual partition, [9,10] obtained the optimal convergence rates in L^2 norm on rectangular meshes, and the results were extended to h^2-parallelogram meshes in [11]. After that, according to the research for any order finite volume element schemes on quadrilateral meshes [12,13], we can find the theoretical analysis of quadratic FVEM was further improved for $h^{1+\gamma}$-parallelogram meshes. In addition, recent research has extended the quadratic FVEM to tetrahedral and cuboid meshes for three-dimensional problems (e.g. [16,17]).

For 2D problem, it's worth noting that all the above finite volume element schemes are constructed on triangular and quadrilateral meshes. We know more and more numerical schemes are constructed on polygonal and polyhedral meshes (e.g. [19–23]), however, there is little research on finite volume element scheme over polygonal meshes currently. Recently, a linear FVEM for arbitrary convex polygonal meshes was proposed in [18], and the optimal H^1 error estimate was obtained under some geometric assumptions and coercivity assumptions. To the best of our knowledge, no previous study presented the quadratic FVEM on polygonal meshes. Therefore, the focus of our research interest is constructing and analyzing the quadratic FVEM over arbitrary convex polygonal meshes.

When we obtain shape functions with quadratic precision by the pairwise products of generalized barycentric coordinates over a general polygonal cell, we find it will lead into some additional degrees of freedom inside the cell. However, the interior unknowns will produce great difficulties for constructing unified dual partitions on arbitrary polygonal meshes, and maybe it can only be done case by case (e.g. triangular meshes, quadrilateral meshes, pentagonal meshes …). Fortunately, we find some research about quadratic serendipity element shape functions over arbitrary polygonal meshes. The authors of [24] established the quadratic serendipity finite element method on polygonal meshes by using generalized barycentric coordinates, and what was more, other constructions of quadratic serendipity finite element method can be found in [25–28]. By using mean value coordinate, [29] offered a simple and efficient method to explicitly construct quadratic serendipity element shape functions on both convex and concave polygons. From the above research results, the quadratic serendipity elements only need $2n$ basis functions for n-sided polygon, associated with vertices and edge midpoints to achieve quadratic precision. The number of basis functions reduces from $n(n+1)/2$ to $2n$, which contributes to establish unified quadratic FVEM.

Based on the quadratic serendipity element using Wachspress coordinate, we construct the quadratic serendipity finite volume element scheme over arbitrary convex polygonal meshes, which has fewer degrees of freedom, and find the scheme on triangular meshes can reduce to the P_2 finite volume element scheme with parameters (α,β), e.g. [1–6]. Then, we obtain some coercivity results for certain special cases and optimal H^1 error estimate, and show some numerical results for solving the anisotropic diffusion problem on convex polygonal meshes.

The remainder of this article is organized as follows. We introduce some notations about the primary and dual meshes and the construction of quadratic serendipity element shape functions using Wachspress coordinate in Section 2, and present the quadratic serendipity polygonal finite volume element method. In Section 3, we obtain the optimal H^1 error estimate for the quadratic serendipity polygonal finite volume element scheme. Some numerical results on several polygonal meshes are shown in Section 4, which verifies our theoretical analysis. Finally, we conclude the article in Section 5.

2   Quadratic serendipity polygonal finite volume element method

In this article, we consider the anisotropic diffusion equation

$$-\nabla\cdot(\Lambda\nabla u)=f, \quad \text{in } \Omega, \tag{2.1}$$

$$u=0, \quad \text{on } \partial\Omega, \tag{2.2}$$

where Ω is an open bounded polygonal domain in $\mathbb{R}^2$. $f\in L^2(\Omega)$ is the source term. Λ is a symmetric, positive-definite and piecewise smooth tensor-valued function, thus, for generic positive constants $\underline{\lambda}$ and $\overline{\lambda}$, it satisfies

$$\underline{\lambda}\|\boldsymbol{x}\|^2 \leq \boldsymbol{x}^T\Lambda\boldsymbol{x} \leq \overline{\lambda}\|\boldsymbol{x}\|^2, \quad \forall \boldsymbol{x}\in\mathbb{R}^2,$$

where $\|\cdot\|$ denotes the Euclidean norm in $\mathbb{R}^2$. Then, we introduce the following notations and assumptions for the primary mesh $\mathcal{T}_h$ of Ω.

- $\mathcal{M}$ denotes the set of disjoint polygonal cells, satisfying $\overline{\Omega}=\cup_{K\in\mathcal{M}}\overline{K}$ where K is a generic cell in $\mathcal{M}$. We know K is an open and connected subset of Ω. We assume that K is strictly convex in the sense that all interior angles of K are less than π, and denote by $\boldsymbol{x}_K$ its averaging center. The measure, diameter of K and the radius of the largest circle inscribed in K are denoted as $|K|$, h_K and ρ_K, respectively. Let $h=\max_{K\in\mathcal{M}}h_K$.

- $\mathcal{V}$ denotes the set of vertices, where $\boldsymbol{v}\in\mathcal{V}$ is a vertex of the cell $K\in\mathcal{M}$.

- $\mathcal{N}$ denotes the set of edge midpoints, where $\boldsymbol{m}\in\mathcal{N}$ is a edge midpoint of the cell $K\in\mathcal{M}$. Let $\mathcal{W}=\mathcal{V}\cup\mathcal{N}$, $\mathcal{W}^{int}=\mathcal{W}\cap\Omega$.
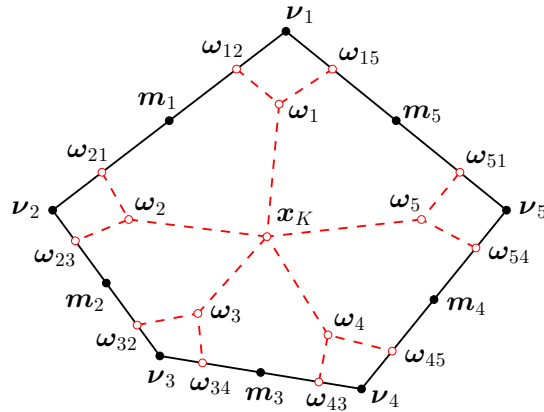
Figure 1: The primary cell (black solid line) and dual cell (red dashed line).

Here we assume that the primary mesh is conforming, which means the intersection of the enclosures of any two cells in $\mathcal{M}$ is either empty or a common vertex or a common edge. Let $\mathbf{v}_1, \mathbf{v}_2, \cdots, \mathbf{v}_n$ denote the vertices of K, and $\mathbf{m}_1, \mathbf{m}_2, \cdots, \mathbf{m}_n$ denote the edge midpoints of K. The averaging center $\mathbf{x}_K$ is defined as

$$\mathbf{x}_K = \frac{1}{n} \sum_{i=1}^{n} \mathbf{v}_i. \tag{2.3}$$

For k is a periodic index with period n, we define that $\boldsymbol{\omega}_{k,k+1}$ and $\boldsymbol{\omega}_{k+1,k}$ are two points on the edge $\mathbf{v}_k \mathbf{v}_{k+1}$, and $\boldsymbol{\omega}_k$ is a point on the edge $\mathbf{v}_k \mathbf{x}_K$, satisfying

$$\alpha := \frac{|\mathbf{v}_k \boldsymbol{\omega}_{k,k+1}|}{|\mathbf{v}_k \mathbf{v}_{k+1}|} = \frac{|\boldsymbol{\omega}_{k+1,k} \mathbf{v}_{k+1}|}{|\mathbf{v}_k \mathbf{v}_{k+1}|} \in \left(0, \frac{1}{2}\right), \quad \beta := \frac{|\mathbf{v}_k \boldsymbol{\omega}_k|}{|\mathbf{v}_k \mathbf{x}_K|} \in (0,1). \tag{2.4}$$

For each vertex $\mathbf{v} \in \mathcal{V}$ and each edge midpoint $\mathbf{m} \in \mathcal{N}$, we associate them with the dual cells $D_{\mathbf{v}}^*$ and $D_{\mathbf{m}}^*$. For example, we plot a pentagonal cell in Fig. 1. All dual cells constitute the dual mesh $\mathcal{T}_h^*$, i.e., $\mathcal{T}_h^* := \{D_{\mathbf{v}}^* : \mathbf{v} \in \mathcal{V}\} \cup \{D_{\mathbf{m}}^* : \mathbf{m} \in \mathcal{N}\} = \{D_{\mathbf{v}}^* : \mathbf{v} \in \mathcal{W}\}$.

2.1 Generalized barycentric coordinate

The generalized barycentric coordinate shape functions are defined by

$$\phi_i(\mathbf{x}) = \frac{w_i(\mathbf{x})}{\sum_{j=1}^{n} w_j(\mathbf{x})}, \quad \mathbf{x} \in K, \tag{2.5}$$

where $w_i(\mathbf{x})$ are the weight functions, and we know the different weight functions can lead to the different generalized barycentric coordinate (GBC) shape functions [30,31], such as Wachspress coordinate [32], mean value coordinate [33] and so on. In this article, we use the Wachspress coordinate to obtain the following quadratic serendipity

element shape functions. From [32], the weight functions of Wachspress coordinate are defined as

$$w_i(x) = A_i(v_{i-1}) \prod_{1 \le j \le n, \ j \ne i-1, i} A_j(x), \quad i = 1, \cdots, n, \tag{2.6}$$

or

$$w_i(x) = \frac{A_i(v_{i-1})}{A_{i-1}(x) A_i(x)}, \quad i = 1, \cdots, n, \tag{2.7}$$

where $A_i(x)$, $x \in K$ denotes the area of the triangle with vertices x, v_i and v_{i+1}, and i is a periodic index with period n such that $v_0 = v_n$, $v_{n+1} = v_1$. Both definitions of the weight functions in (2.6) and (2.7) lead to the same Wachspress shape functions by (2.5). In this article, we use the definition in (2.6), because it allows the direct evaluation of shape functions up to the cell boundary.

2.2 The construction of quadratic serendipity element shape functions

As we all known, the generalized barycentric coordinates are only guaranteed to have linear precision. Then we use the pairwise products of generalized barycentric coordinates to obtain the following constant, linear, and quadratic precision,

$$\sum_i \varphi_i(x) = 1, \quad \sum_i v_i \varphi_i(x) = x, \quad \sum_i v_i v_i^T \varphi_i(x) = x x^T.$$

The construction of quadratic serendipity element (QSE) shape functions on a polygonal cell includes three steps [24, 29]: order elevation, function reduction, and Lagrange property preservation,

$$\{\phi_i\} \xrightarrow{\text{Order elevation}} \{\chi_{i,j}\} \xrightarrow[\text{Linear transformation } \mathbb{A}]{\text{Function reduction}} \{\psi_{i,i}, \psi_{i,i+1}\} \xrightarrow[\text{Linear transformation } \mathbb{B}]{\text{Lagrange property preservation}} \{\varphi_i, \varphi_{n+i}\}$$

where $j \ge i$, $i, j = 1, 2, \cdots, n$, as follows.

- (Order elevation) We define $\chi_{i,j} := \phi_i \phi_j$, $j \ge i$, $i, j = 1, 2, \cdots, n$, where ϕ_i is defined in (2.5) and (2.6).

- (Function reduction [29]) We obtain $2n$ quadratic functions $\{\psi_{i,i}, \psi_{i,i+1}\}$, $i = 1, 2, \cdots, n$ as follows,

$$\begin{cases} \psi_{i,i} = \chi_{i,i} + \sum_{j \ne \{i-1, i, i+1\}} a_{i,j}^{i,i} \chi_{i,j}, \\ \psi_{i,i+1} = \chi_{i,i+1} + \sum_{j \ne \{i-1, i, i+1\}} a_{i,j}^{i,i+1} \chi_{i,j} + \sum_{j \ne \{i, i+1, i+2\}} a_{i+1,j}^{i+1,i} \chi_{i+1,j}, \end{cases}$$

where $\chi_{i,j} = \chi_{j,i}$, and

$$a_{i,j}^{i,i} = -A_{i-1,i+1,j} / A_{i-1,i,i+1}, \ a_{i,j}^{i,i-1} = A_{j,i,i+1} / (2 A_{i-1,i,i+1}), \ a_{i,j}^{i,i+1} = A_{i-1,i,j} / (2 A_{i-1,i,i+1}).$$

- (Lagrange property preservation) The $2n$ QSE shape functions $\{\varphi_i, \varphi_{n+i}\}$, $i = 1, 2, \cdots, n$ are obtained by $\varphi_i = \psi_{i,i} - \psi_{i,i+1} - \psi_{i-1,i}$, $\varphi_{n+i} = 4 \psi_{i,i+1}$.
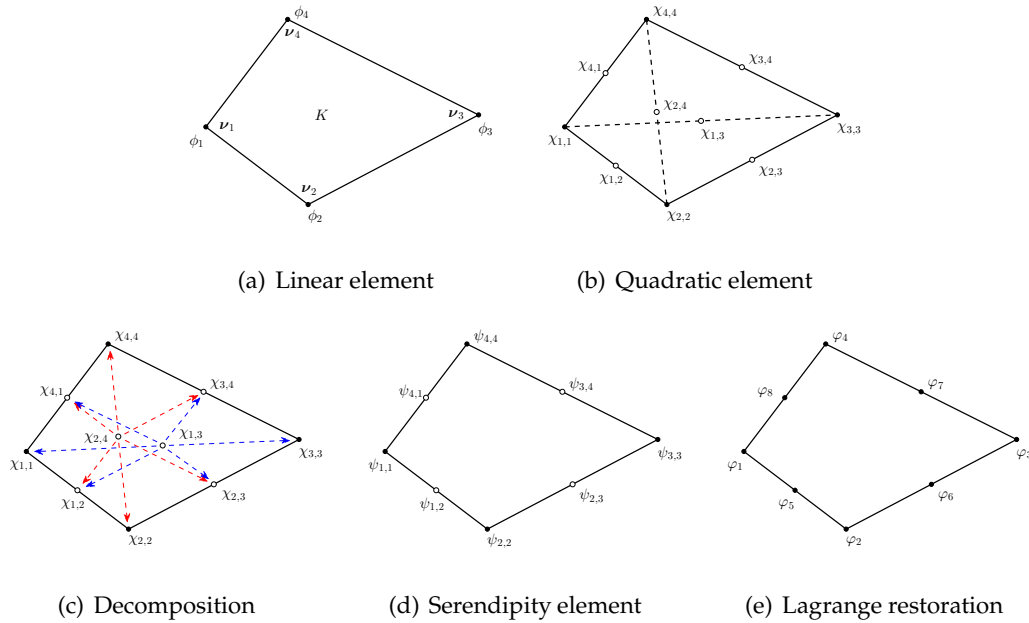
(a) Linear element   (b) Quadratic element

(c) Decomposition   (d) Serendipity element   (e) Lagrange restoration

Figure 2: The construction of QSE shape functions for a quadrilateral cell.

$A_{i,j,k}$ denotes the area of triangle $\nu_i\nu_j\nu_k$, and $\psi_{n,n+1} = \psi_{n,1}$. As a note, $\psi_{i,i}$, φ_i and $\psi_{i,i+1}$, φ_{n+i} are associated with the vertex ν_i and the edge midpoint m_i.

In order to describe the construction process of QSE shape functions carefully, we give an example for a quadrilateral cell K with vertices ν_1, ν_2, ν_3, ν_4 in Algorithm 1.

Algorithm 1: The construction of QSE shape functions for a quadrilateral cell

---

Step 0: Get the linear generalized barycentric coordinate shape functions $\{\phi_i\}$, which are defined in (2.5) and (2.6), see Fig. 2(a);

Step 1: Obtain $n(n+1)/2 = 10$ unique functions $\{\chi_{i,j}\}$ by pairwise multiplying $\{\phi_i\}$, see Fig. 2(b);

Step 2: Split each function $\chi_{i,j}$, $j \neq i, i+1$ up into six functions, see Fig. 2(c), and add them to functions $\chi_{i,i}$, $\chi_{j,j}$, $\chi_{i-1,i}$, $\chi_{i,i+1}$, $\chi_{j-1,j}$, $\chi_{j,j+1}$ to obtain $2n = 8$ functions $\{\psi_{i,i}, \psi_{i,i+1}\}$, see Fig. 2(d);

Step 3: Compute $2n = 8$ QSE shape functions $\{\varphi_i\}$ for Lagrange property preservation, see Fig. 2(e).

2.3 Quadratic serendipity polygonal finite volume element equation

We choose the trial function space as $U_h = \mathrm{Span}\{\varphi_v : v \in \mathcal{W}^{int}\}$, where φ_v denotes the quadratic serendipity element shape function, which is introduced in Subsection 2.2,

and the test function space as

$$V_h = \{v_h \in L^2(\bar{\Omega}) : v_h|_{D^*_v} = constant, \ \forall \ \boldsymbol{v} \in \mathcal{W}^{int}; \ v_h|_{D^*_v} = 0, \ \forall \ \boldsymbol{v} \in \mathcal{W} \cap \partial \Omega\},$$

where the two parameters of dual partition α, β are defined as (2.4). Then we propose the quadratic serendipity polygonal finite volume element method (QS−PFVEM) to solve this problem, where the numerical solution $u_h \in U_h$ satisfying

$$- \sum_{\boldsymbol{v} \in \mathcal{W}^{int}} v_h(\boldsymbol{v}) \oint_{\partial D^*_v} (\Lambda \nabla u_h) \cdot \boldsymbol{n} \, \mathrm{d}s = \sum_{\boldsymbol{v} \in \mathcal{W}^{int}} v_h(\boldsymbol{v}) \int_{D^*_v} f \mathrm{d}x \mathrm{d}y, \quad \forall \boldsymbol{v} \in \mathcal{W}^{int}, \qquad (2.8)$$

where $\boldsymbol{n}$ is the unit normal outward to the dual cell boundary ∂D^*_v.

Remark 2.1. According to the construction of quadratic serendipity element shape functions in Subsection 2.2, we can find QSE shape functions on triangular meshes reduce to the P_2 finite element functions. Thus, QS−PFVEM on triangular meshes reduces to the P_2 finite volume element method (P_2−FVEM) with parameters (α, β), because both of them also use the same dual partition. In other words, the scheme is also regarded as a new development, which extends the P_2−FVEM to polygonal meshes. For the choice of dual partition parameters (α, β) in this article, we recommend the following two schemes. First, QS−PFVEM with $\alpha = (3 - \sqrt{3})/6$, $\beta = (6 + \sqrt{3} - \sqrt{21 + 6\sqrt{3}})/6$ (scheme I) on triangular meshes reduces to the P_2−FVEM in [4], which has optimal H^1 and L^2 convergence orders. Second, QS−PFVEM with $\alpha = (3 - \sqrt{3})/6$, $\beta = (3 - \sqrt{3})/4$ (scheme II) on triangular meshes reduces to the P_2−FVEM in [5], which has been proved that it is unconditionally stable and has optimal H^1 convergence order.

3 H^1 Error estimate

First, we introduce some geometric assumptions for error estimate. Let the vertices of K be denoted by $\boldsymbol{v}_1, \boldsymbol{v}_2, \cdots, \boldsymbol{v}_n$ and the interior angle at $\boldsymbol{v}_i$ be θ_i. Two geometric assumptions for any $K \in \mathcal{M}$ are given, as follows.

- (**G1**) There exists a positive constant d_* such that $\min_{i \neq j} \|\boldsymbol{v}_i - \boldsymbol{v}_j\| > d_* h_K$, where $\|\cdot\|$ denotes the Euclidean norm in $\mathbb{R}^2$.

- (**G2**) There exists a positive constant θ^* such that $\max_{1 \leq i \leq n} \{\theta_i\} < \theta^* < \pi$.

Let $|\cdot|_{m,\mathcal{D}}$ be the semi-norm of Sobolev space $H^m(\mathcal{D})$. Under the geometric constraints (**G1**) and (**G2**), one can obtain the following error estimate. Note that "$A \lesssim B$" denotes that A can be bounded by B multiplied by a constant independent of h, and "$A \gtrsim B$" denotes that B can be bounded by A similarly.

3.1   Interpolation error estimate

Lemma 3.1. *Under the geometric assumptions* (**G1**) *and* (**G2**), *for the quadratic serendipity element shape functions* $\varphi_i(\boldsymbol{x})$, $i=1,2,\cdots,2n$, *we have* $\|\nabla\varphi_i\|\lesssim h_K^{-1}$ *and* $|\varphi_i|_{2,K}\lesssim h_K^{-1}$.

Proof. By the Lemma 4 and Lemma 6 in [18], for the Wachspress coordinate ϕ_i, we know $\|\nabla\phi_i\|\lesssim h_K^{-1}$ and $|\phi_i|_{2,K}\lesssim h_K^{-1}$. According to the definition of generalized barycentric coordinate in (2.5), we have $|\phi_i|<1$. By the chain rule and $\chi_{i,j}=\phi_i\phi_j$, $j\geq i$, $i,j=1,2,\cdots,n$, we have $\|\nabla\chi_{i,j}\|\lesssim h_K^{-1}$ and $|\chi_{i,j}|_{2,K}\lesssim h_K^{-1}$. From the construction of quadratic serendipity element shape functions in Subsection 2.2 and the Theorem 1 of [29], $\{\psi_{i,i},\,\psi_{i,i+1}\}$ and $\{\varphi_i,\,\varphi_{n+i}\}$ are obtained by the bounded linear transformations $\mathbb{A}$ and $\mathbb{B}$ from $\{\chi_{i,j}\}$, so $\|\nabla\varphi_i\|\lesssim h_K^{-1}$ and $|\varphi_i|_{2,K}\lesssim h_K^{-1}$. $\qquad\square$

For the Wachspress coordinate, by the Lemma 6 of [34] and Theorem 1 of [29], we have the H^1 norm of QSE shape functions are uniformly bounded. Then we obtain the following H^1 interpolation error estimate for QSE shape functions in Lemma 3.2 by the Bramble-Hilbert lemma and Sobolev embedding theorem, where the proof of it is similar to the Theorem 5 in [29]. For the H^1 error analysis for QS$-$PFVEM, we also need the H^2 interpolation error estimate for QSE shape functions. By Lemma 3.1, we obtain the following H^2 interpolation error estimate for QSE shape functions in Lemma 3.3, where the proof of it is similar to Theorem 1 in [18].

Lemma 3.2. *Under the geometric constraints* (**G1**) *and* (**G2**), *for all* $u\in H^3(K)$, *we have*

$$|u-u_I|_{1,K}\lesssim h_K^2|u|_{3,K}. \tag{3.1}$$

Lemma 3.3. *Under the geometric constraints* (**G1**) *and* (**G2**), *for all* $u\in H^3(K)$, *we have*

$$|u-u_I|_{2,K}\lesssim h_K|u|_{3,K}. \tag{3.2}$$

3.2   The coercivity result

On triangular meshes, we note that QS$-$PFVEM reduces to the P_2-FVEM with parameters (α,β), which has been studied extensively, e.g. [1–6]. So, in this case the coercivity result of QS$-$PFVEM can be directly obtained from the existing works. Specifically, we have the following result.

Lemma 3.4 ([6], Section 7). *Assume that the diffusion tensor* Λ *is piecewise constant with respect to* $\mathcal{T}_h$, *or* Λ *is piecewise* $W^{1,\infty}$ *and the mesh size* h *is sufficiently small. For the QS$-$PFVEM, if the angles of each triangular cell satisfy the minimum angle conditions in Table* 1, *we have*

$$a_h(u_h,\Pi_h^*u_h)\gtrsim|u_h|_{1,\Omega,h}^2, \quad \forall u_h\in U_h, \tag{3.3}$$

where

$$|v|_{1,\Omega,h}^2=\sum_{K\in\mathcal{M}}|v|_{1,K,h}^2, \quad |v|_{1,K,h}^2=\sum_{i=1}^n(v_{i+1}-v_i)^2,$$

and Π_h^* *is a bijective linear mapping which maps* $u_h\in U_h$ *to* $\Pi_h^*u_h\in V_h$.

Table 1: The existing minimum angle conditions for triangular meshes.

(α,β)	Minimum angle conditions
$(1/3,1/2)$	$10.08°$
$(1/6,3/8)$	$7.11°$
$(1/4,1/2)$	$4.14°$
$((3-\sqrt{3})/6,(6+\sqrt{3}-\sqrt{21+6\sqrt{3}})/6)$	$1.42°$
$((3-\sqrt{3})/6,(3-\sqrt{3})/4)$	Unconditionally stable

Remark 3.1. As for the general polygonal meshes $n \geq 4$, the coercivity analysis is an extremely challenging work, because the quadratic serendipity element shape functions are more complex than the classical P_2 finite element functions, and the corresponding analysis involves too much geometric parameters.

In this paper, we treat the coercivity result for QS$-$PFVEM on general polygonal meshes ($n \geq 4$) as an assumption, as follows.

- (**A1**) The coercivity result of QS$-$PFVEM (3.3) holds for arbitrary convex polygonal meshes.

3.3 An optimal H^1 error estimate

Due to $\|\nabla \varphi_i\| \lesssim h_K^{-1}$ in Lemma 3.1, we have $|u_h|_{1,\Omega} \lesssim |u_h|_{1,\Omega,h}$, $\forall u_h \in U_h$. Then we obtain the following optimal H^1 error estimate for QS$-$PFVEM by the H^1 and H^2 interpolation error estimates in Lemma 3.2 and Lemma 3.3.

Theorem 3.1. *Assume that $\mathcal{T}_h$ consists of arbitrary convex polygons, and the diffusion tensor Λ satisfies the same assumptions in Lemma 3.4. Let u be the exact solution of (2.1) and (2.2), and u_h be the quadratic serendipity polygonal finite volume element solution of (2.8). Then, under the geometric constraints (**G1**), (**G2**) and the coercivity assumption (**A1**), we have*

$$|u-u_h|_{1,\Omega} \lesssim h^2 |u|_{3,\Omega}. \tag{3.4}$$

4 Numerical examples

In this section, we solve two numerical examples on $\Omega = [0,1]^2$ by QS$-$PFVEM. To measure the accuracy and mesh flexibility, four typical mesh types are employed in Fig. 3.

4.1 Example 1

Firstly, we solve the example with the following diffusion tensor and exact solution,

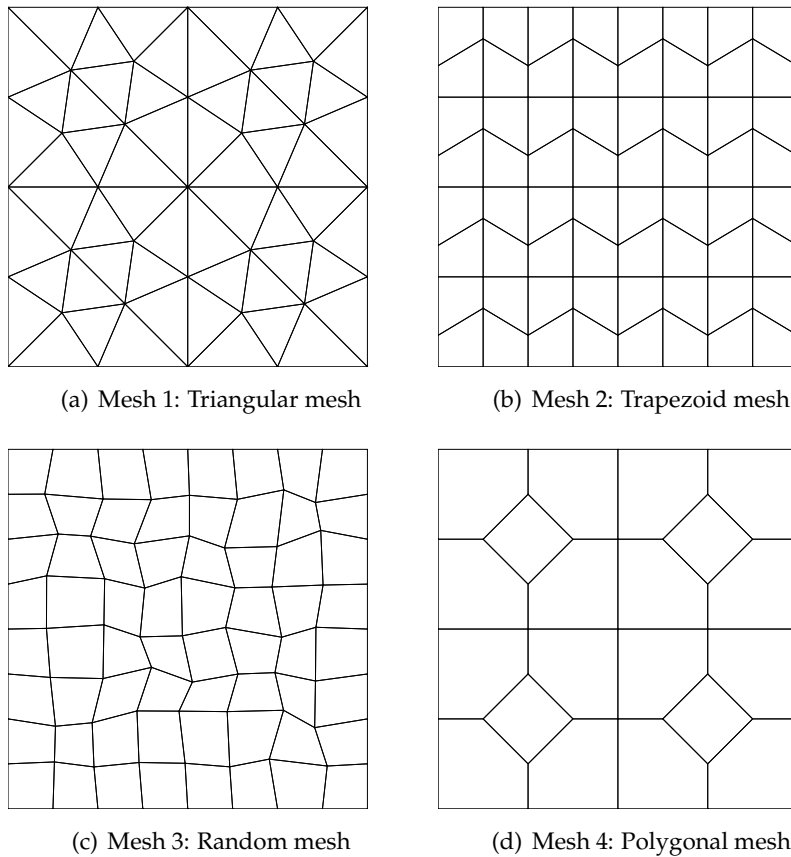$$\Lambda = \begin{pmatrix} 1.0 & 0.2 \\ 0.2 & 0.5 \end{pmatrix}, \quad u(x,y) = e^{0.1x+0.2y}.$$

(a) Mesh 1: Triangular mesh (b) Mesh 2: Trapezoid mesh

(c) Mesh 3: Random mesh (d) Mesh 4: Polygonal mesh

Figure 3: Mesh types used in the numerical tests.

For the example, we compute H^1 errors E_q and convergence rates R_q for two schemes, scheme I with parameters $\alpha = (3-\sqrt{3})/6$, $\beta = (6+\sqrt{3}-\sqrt{21+6\sqrt{3}})/6$ in Table 2, and scheme II with parameters $\alpha = (3-\sqrt{3})/6$, $\beta = (3-\sqrt{3})/4$ in Table 3. We can find that the convergence rates of H^1 errors are optimal on the four polygonal meshes, which verifies the previously discussed theorem of error estimate in Theorem 3.1. From the numerical tests, we observe that the quadratic serendipity polygonal finite volume element method is coercive for these numerical experiments.

Moreover, we also care about L^2 errors E_u and convergence rates R_u, and the numerical results of scheme I are shown in Table 4. Unfortunately, the convergence orders of L^2 errors are 3 only for the triangular meshes, since we know the scheme I on triangular meshes reduces to the P_2-FVEM in [4] with the optimal L^2 error estimate, but others are nearly one order lower than the optimal convergence order asymptotically. For the scheme II, the convergence orders of L^2 errors are all asymptotically 2 on these polygonal meshes in Table 5. We note that QS−PFVEM on rectangular meshes reduces to the conventional eight-nodes serendipity finite volume element method. In [35], some numerical results for the conventional eight-nodes serendipity finite volume element

Table 2:   The H^1 errors and convergence rates of scheme I for Example 1.

Mesh		level 1	level 2	level 3	level 4	level 5
	h	2.50000E-01	1.25000E-01	6.25000E-02	3.12500E-02	1.56250E-02
Mesh 1	E_q	2.57452E-06	6.68319E-07	1.70085E-07	4.28928E-08	1.07694E-08
	R_q		1.94569	1.97428	1.98745	1.99380
	h	2.05015E-01	1.02508E-01	5.12538E-02	2.56269E-02	1.28135E-02
Mesh 2	E_q	2.53836E-06	6.75835E-07	1.74228E-07	4.42217E-08	1.11389E-08
	R_q		1.90915	1.95570	1.97815	1.98915
	h	2.30833E-01	1.13773E-01	5.90181E-02	3.01534E-02	1.50528E-02
Mesh 3	E_q	1.47079E-06	4.34468E-07	1.09103E-07	2.89859E-08	7.30799E-09
	R_q		1.72360	2.10530	1.97377	1.98327
	h	3.53553E-01	1.76777E-01	8.83883E-02	4.41942E-02	2.20971E-02
Mesh 4	E_q	2.31334E-06	5.41486E-07	1.30940E-07	3.21906E-08	7.98022E-09
	R_q		2.09498	2.04802	2.02420	2.01214

Table 3:   The H^1 errors and convergence rates of scheme II for Example 1.

Mesh		level 1	level 2	level 3	level 4	level 5
	h	2.50000E-01	1.25000E-01	6.25000E-02	3.12500E-02	1.56250E-02
Mesh 1	E_q	2.72995E-06	7.10795E-07	1.81142E-07	4.57115E-08	1.14809E-08
	R_q		1.94137	1.97231	1.98649	1.99333
	h	2.05015E-01	1.02508E-01	5.12538E-02	2.56269E-02	1.28135E-02
Mesh 2	E_q	1.91110E-06	5.11786E-07	1.32319E-07	3.36329E-08	8.47774E-09
	R_q		1.90079	1.95152	1.97608	1.98812
	h	2.30833E-01	1.13773E-01	5.90181E-02	3.01534E-02	1.50528E-02
Mesh 3	E_q	1.23250E-06	3.66832E-07	9.20063E-08	2.44739E-08	6.15927E-09
	R_q		1.71294	2.10716	1.97194	1.98588
	h	3.53553E-01	1.76777E-01	8.83883E-02	4.41942E-02	2.20971E-02
Mesh 4	E_q	1.86785E-06	4.31675E-07	1.03723E-07	2.54181E-08	6.29119E-09
	R_q		2.11336	2.05721	2.02880	2.01445

method on rectangular meshes were shown that the convergence orders of L^2 errors are only 2, which are one order lower than the optimal order. According to the development of P_2-FVEM and conventional eight-nodes serendipity finite volume element method, the optimal L^2 error estimate is very sensitive to selection of dual partitions. Finding one unified dual partition to obtain the optimal convergence order of L^2 errors is our future work emphasis.

Table 4:   The L^2 errors and convergence rates of scheme I for Example 1.

Mesh		level 1	level 2	level 3	level 4	level 5
Mesh 1	h	2.50000E-01	1.25000E-01	6.25000E-02	3.12500E-02	1.56250E-02
	E_u	1.40988E-07	1.75254E-08	2.18526E-09	2.72847E-10	3.40874E-11
	R_u		3.00805	3.00357	3.00164	3.00078
Mesh 2	h	2.05015E-01	1.02508E-01	5.12538E-02	2.56269E-02	1.28135E-02
	E_u	5.24931E-08	6.52632E-09	8.99955E-10	1.63678E-10	3.83202E-11
	R_u		3.00778	2.85835	2.45899	2.09468
Mesh 3	h	2.30833E-01	1.13773E-01	5.90181E-02	3.01534E-02	1.50528E-02
	E_u	4.82800E-08	6.83671E-09	1.12291E-09	2.15990E-10	5.58851E-11
	R_u		2.76287	2.75213	2.45470	1.94598
Mesh 4	h	3.53553E-01	1.76777E-01	8.83883E-02	4.41942E-02	2.20971E-02
	E_u	2.26644E-07	3.23707E-08	5.19135E-09	1.02414E-09	2.35407E-10
	R_u		2.80767	2.64050	2.34170	2.12119

Table 5:   The L^2 errors and convergence rates of scheme II for Example 1.

Mesh		level 1	level 2	level 3	level 4	level 5
Mesh 1	h	2.50000E-01	1.25000E-01	6.25000E-02	3.12500E-02	1.56250E-02
	E_u	1.39371E-07	1.74231E-08	2.20393E-09	2.89291E-10	4.23749E-11
	R_u		2.99986	2.98285	2.92949	2.77124
Mesh 2	h	2.05015E-01	1.02508E-01	5.12538E-02	2.56269E-02	1.28135E-02
	E_u	4.88395E-08	6.08073E-09	8.10819E-10	1.36675E-10	3.05294E-11
	R_u		3.00573	2.90679	2.56863	2.16248
Mesh 3	h	2.30833E-01	1.13773E-01	5.90181E-02	3.01534E-02	1.50528E-02
	E_u	4.45674E-08	6.37989E-09	1.02525E-09	1.92389E-10	5.07172E-11
	R_u		2.74753	2.78539	2.49152	1.91910
Mesh 4	h	3.53553E-01	1.76777E-01	8.83883E-02	4.41942E-02	2.20971E-02
	E_u	2.24720E-07	3.19788E-08	5.03216E-09	9.71010E-10	2.20634E-10
	R_u		2.81294	2.66786	2.37362	2.13783

4.2   Example 2

Secondly, we consider the discontinuous diffusion tensor with one discontinuity line $x=1/2$, where the diffusion tensor and the exact solution are given as follows,

$$\Lambda = \begin{cases} \Lambda_1, & 0 \leq x \leq 0.5, \\ \Lambda_2, & 0.5 < x \leq 1, \end{cases} \quad \Lambda_1 = \begin{pmatrix} 10 & 2 \\ 2 & 5 \end{pmatrix}, \quad \Lambda_2 = \begin{pmatrix} 1 & 0 \\ 0 & 1 \end{pmatrix},$$
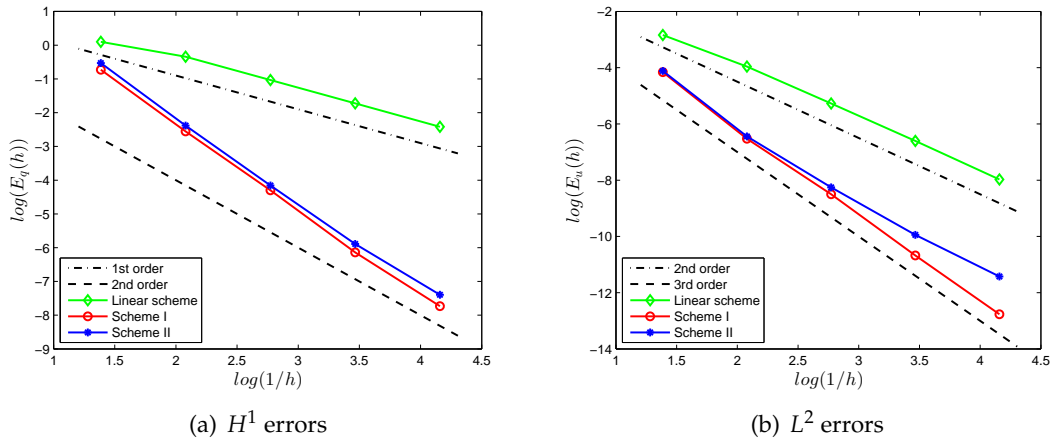
(a) H^1 errors　　　　　　　　　　　(b) L^2 errors

Figure 4: The numerical results on Mesh 1 for Example 2.

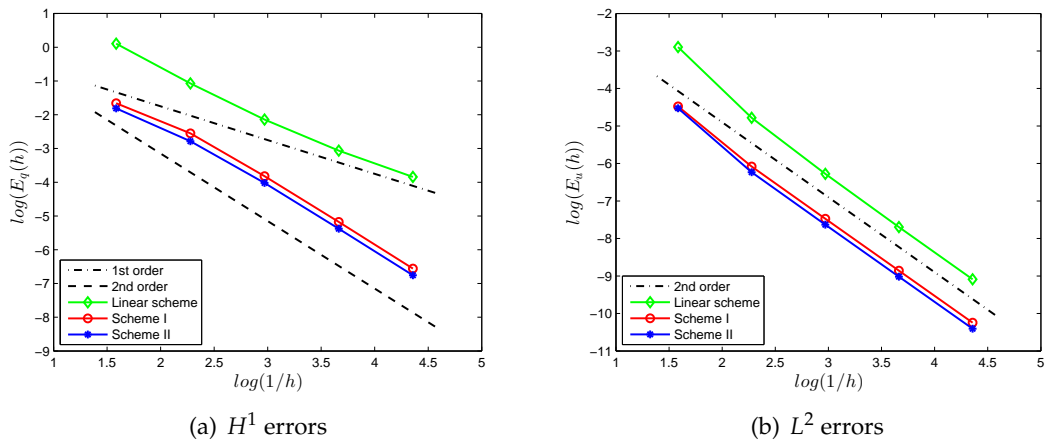(a) H^1 errors　　　　　　　　　　　(b) L^2 errors

Figure 5: The numerical results on Mesh 2 for Example 2.

$$u(x,y)=\begin{cases} \left[(x-0.5)(8\pi(y-0.5)+0.1)+1\right]e^{-20\pi(y-0.5)^2}, & 0\leq x\leq 0.5, \\ e^{x-20\pi(y-0.5)^2-0.5}, & 0.5<x\leq 1. \end{cases}$$

We solve the problem by the linear FVEM scheme on polygonal meshes in [18] (linear scheme), and two quadratic serendipity polygonal finite volume element schemes (scheme I and scheme II), and draw log-log plots of the H^1 errors and L^2 errors with mesh size h in Figs. 4, 5, 6. One can observe that the numerical performance is similar to Example 1, and the optimal convergence orders of H^1 errors are obtained for the scheme I and scheme II.
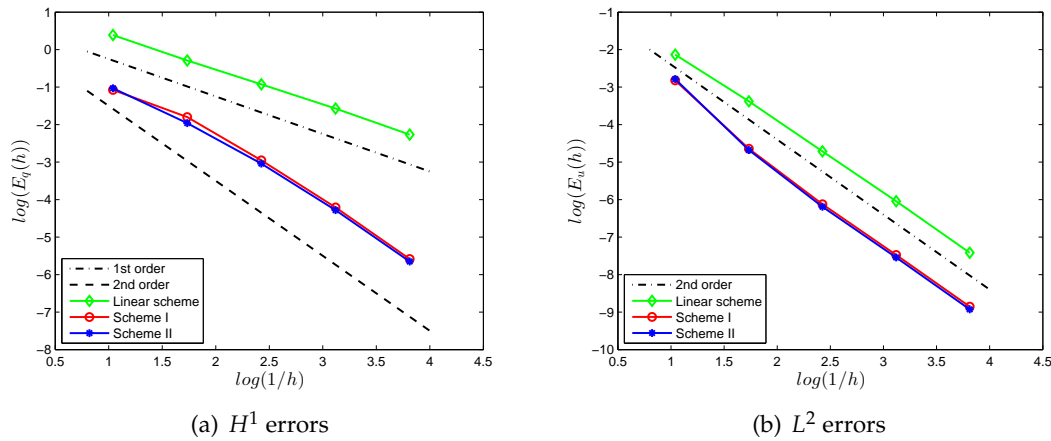
(a) H^1 errors   (b) L^2 errors

Figure 6: The numerical results on Mesh 4 for Example 2.

5 Conclusion

Thanks to the quadratic serendipity element, we propose the quadratic serendipity finite volume element scheme for solving the anisotropic diffusion problem on arbitrary convex polygonal meshes. The trial function space is constructed by explicit quadratic serendipity element shape functions based on Wachspress coordinate, and we present a family of unified dual partitions for arbitrary convex polygonal meshes. The scheme reduces to the P_2 finite volume element method on triangular meshes, and it reduces to the conventional eight-nodes serendipity finite volume element method on rectangular meshes. Moreover, we analyze that the scheme has optimal H^1 error estimate on convex polygonal meshes, and verify it by some numerical examples. In the future, we will investigate the coercivity and L^2 error estimate, and construct one quadratic finite volume element scheme on arbitrary convex polygonal meshes with optimal convergence orders both under H^1 and L^2 norms.

Acknowledgments

References

[1] M. Tian and Z. Chen, Quadratic element generalized differential methods for elliptic equations, Numer. Math. J. Chin. Univ., 13 (1991), 99-113.

[2] P. Emonot, Methodes de volumes elements finis: Applications aux equations de Navier Stokes et resultats de convergence, PhD Dissertation, Lyon, 1992.

[3] F. Liebau, The finite volume element method with quadratic basis functions, Computing, 57 (1996), 281-299.

[4] X. Wang and Y. Li, L^2 error estimates for high order finite volume methods on triangular meshes, SIAM J. Numer. Anal., 54 (2016), 2729-2749.

[5] Q. Zou, An unconditionally stable quadratic finite volume scheme over triangular meshes for elliptic equations, J. Sci. Comput., 70 (2017), 112-124.

[6] Y. Zhou and J. Wu, A unified analysis of a class of quadratic finite volume element schemes on triangular meshes, Adv. Comput. Math., 46 (2020), 1-31.

[7] X. Xiang, Generalized difference methods for second order elliptic equations, Numer. Math. J. Chinese Univ., 2 (1983), 114-126.

[8] M. Yang, A second-order finite volume element method on quadrilateral meshes for elliptic equations, ESAIM: M2AN, 40 (2006), 1053-1067.

[9] C. Yu and Y. Li, Biquadratic element finite volume method based on optimal stress points for solving Poisson equations, Math. Numer. Sin., 32 (2010), 59-74.

[10] T. Wang and Y. Gu, Superconvergent biquadratic finite volume element method for two-dimensional Poisson's equations, J. Comput. Appl. Math., 234 (2010), 447-460.

[11] J. Lv and Y. Li, Optimal biquadratic finite volume element methods on quadrilateral meshes, SIAM J. Numer. Anal., 50 (2012), 2379-2399.

[12] Z. Zhang and Q. Zou, Vertex-centered finite volume schemes of any order over quadrilateral meshes for elliptic boundary value problems, Numer. Math., 130 (2015), 363-393.

[13] Y. Lin, M. Yang and Q. Zou, L^2 error estimates for a class of any order finite volume schemes over quadrilateral meshes, SIAM J. Numer. Anal., 53 (2015), 2030-2050.

[14] X. Wang and Y. Zhang, On the construction and analysis of finite volume element schemes with optimal L^2 convergence rate, Numer. Math. Theor. Meth. Appl., 14 (2021), 47-70.

[15] A. Li, H. Yang, Y. Li and G. Yuan, The corrected finite volume element methods for diffusion equations satisfying discrete extremum principle, Commun. Comput. Phys., 32 (2022), 1437-1473.

[16] P. Yang, X. Wang and Y. Li, Construction and analysis of the quadratic finite volume methods on tetrahedral meshes, Sci. China Math., 66 (2023), 855-886.

[17] M. Yang, L^2 error estimation of a quadratic finite volume element method for pseudo-parabolic equations in three spatial dimensions, Appl. Math. Comput., 218 (2012), 7270-7278.

[18] Y. Zhou, Y. Zhang and J. Wu, A polygonal finite volume element method for anisotropic diffusion problems, Comput. Math. Appl., 140 (2023), 225-236.

[19] J. Wu, Vertex-centered linearity-preserving schemes for nonlinear parabolic problems on polygonal grids, J. Sci. Comput., 71 (2017) 499-524.

[20] S. Su, H. Tang and J. Wu, An efficient positivity-preserving finite volume scheme for the nonequilibrium three-temperature radiation diffusion equations on polygonal meshes, Commun. Comput. Phys., 30 (2021), 448-485.

[21] J. Xu, F. Zhao, Z. Sheng and G. Yuan, A nonlinear finite volume scheme preserving maximum principle for diffusion equations, Commun. Comput. Phys., 29 (2021), 747-766.

[22] Q. Dong, S. Su and J. Wu, A decoupled and positivity-preserving DDFV scheme for diffusion problems on polyhedral meshes, Commun. Comput. Phys., 27 (2020), 1378-1412.

[23] M. Liu, S. Shu, G. Yuan and X. Yue, Two nonlinear positivity-preserving finite volume schemes for three-dimensional heat conduction equations on general polyhedral meshes, Commun. Comput. Phys., 30 (2021), 1185-1215.

[24] A. Rand, A. Gillette and C. Bajaj, Quadratic serendipity finite elements on polygons using

generalized barycentric coordinates, Math. Comput., 83 (2014), 2691-2716.

[25] N. Sukumar, Quadratic maximum-entropy serendipity shape functions for arbitrary planar polygons, Comput. Methods Appl. Mech. Engrg., 263 (2013), 27-41.

[26] M. Floater and M. Lai, Polygonal spline spaces and the numerical solution of the Poisson equation, SIAM J. Numer. Anal., 54 (2016), 797-824.

[27] A. Sinu, S. Natarajan and K. Shankar, Quadratic serendipity finite elements over convex polyhedra, Int. J. Numer. Meth. Engng., 113 (2018), 109-129.

[28] J. Cao, Y. Xiao, Z. Chen, W. Wang and C. Bajaj, Functional data approximation on bounded domains using polygonal finite elements, Comput. Aided Geom. Des., 63 (2018), 149-163.

[29] J. Cao, Y. Xiao, Y. Xiao, Z. Chen, F. Xue, X. Wei and Y. Zhang, Quadratic serendipity element shape functions on general planar polygons, Comput. Methods Appl. Mech. Engrg., 392 (2022), 114703.

[30] M. Floater, Generalized barycentric coordinates and applications, Acta Numer., 24 (2015), 161-214.

[31] K. Hormann and N. Sukumar, Generalized Barycentric Coordinates in Computer Graphics and Computational Mechanics, CRC Press, Boca Raton, 2017.

[32] E. Wachspress, A Rational Finite Element Basis, Academic Press, New York, 1975.

[33] M. Floater, Mean value coordinates, Comput. Aided Geom. Des., 20 (2003), 19-27.

[34] A. Gillette, A. Rand and C. Bajaj, Error estimates for generalized barycentric interpolation, Adv. Comput. Math., 37 (2012), 417-439.

[35] Y. Zhou and Q. Zou, Locally conservative serendipity finite element solutions for elliptic equations, Int. J. Numer. Anal. Model., 18 (2021), 19-37.